engineering proceedings

MDPI

Proceeding Paper

The Influence of Location of Coanda Surface Ribs on Fluidic Oscillator Performance †

Liaqat Hussain * and Muhammad Mahabat Khan

Department of Mechanical Engineering, Capital University of Science and Technology, Islamabad 45750, Pakistan; mahabat83@yahoo.com

* Correspondence: liaqat.engr@yahoo.com

† Presented at the 4th International Conference on Advances in Mechanical Engineering (ICAME-24), Islamabad, Pakistan, 8 August 2024.

Abstract: Double feedback fluidic oscillators, which create oscillating fluid jets, are commonly used in flow control and thermal applications. The geometry of the Coanda surface affects the oscillation frequency, jet deflection angle, and pressure drop in the mixing chamber. This study numerically investigates the impact of rib locations on the Coanda surface on jet characteristics. Air, with an inlet velocity of 55.8 m/s, is used as the working fluid. Three cases—full ribs, upper ribs, and lower ribs—are compared to a smooth Coanda surface. The full ribs case achieves an increased oscillation frequency of 820 Hz, compared to 355 Hz for the smooth case. However, the jet deflection angles decrease when ribs are present. The upper ribs case achieves a larger 41.5° deflection angle, while the full ribs case achieves a relatively lower 33.8° angle. Interestingly, adding ribs to the Coanda surface reduces the pressure drop in the oscillator. Oscillators with upper ribs achieve a 76.1% increase in FDPR compared to smooth cases, making them the best solution for enhancing the combined effect of jet oscillation frequency and deflection angle.

Keywords: fluidic oscillator; Coanda surface; jet oscillation frequency; jet deflection angle; pressure drop

Citation: Hussain, L.; Khan, M.M. The Influence of Location of Coanda Surface Ribs on Fluidic Oscillator Performance. *Eng. Proc.* **2024**, *75*, 3. https://doi.org/10.3390/engproc2024075003

Academic Editors: Muhammad Irfan, Mohammad Javed Hyder and Manzar Masud

Published: 19 September 2024

1. Introduction

The fluidic oscillator is a significant device used for flow control and other engineering applications. It has no moving part and is known for producing high-frequency oscillating jets. Its simple design and potential for flow control and heat transfer enhancement have driven the interest of researchers since the 1950s. A fluidic oscillator works based on self-sustained instabilities that produce an oscillatory jet. The frequency of the oscillating jet is mainly determined by the flow rate and design of the fluidic oscillator. The fluidic oscillators are divided into three primary types: zero-feedback oscillators [1], single-feedback oscillators [2], and double-feedback [3] oscillators.

The zero-feedback oscillator produces a sweeping jet through shear layers in the mixing chamber. Single-feedback oscillators use one feedback loop to pull the jet to the opposite side. Double-feedback oscillators, based on the Stouffer patent [4], utilize two feedback loops to create a sweeping jet. Double-feedback fluidic oscillators produce unstable sweeping jets with applications in numerous fields, like flow control [5], separation control [6], acoustic control [7], flow measurement [8], and flow mixing enhancement [9]. Recently, they have been used to improve heat transfer rates from hot surfaces [10]. The Coanda effect plays a significant role in the double-feedback oscillator's mechanism, where fluid switches from one side to the other, creating self-sustained oscillatory jets.

Factors such as oscillation frequency, jet deflection angle, and pressure loss, all of which are dependent on the oscillator's internal geometry, influence the choice of a fluidic oscillator for a specific application. Researchers investigated different geometrical variations to see how they affect these factors. In this regard, Bobusch et al. [11] found that the feedback channel width significantly increases oscillation frequency while studying

the impact of varying widths of the mixing chamber inlet and exit nozzle, in addition to varying feedback channel widths, feedback channel lengths, and shapes. Similarly, Baghaei et al. [12] noted that varying the feedback channel width improved the oscillating jet's frequency during the investigation of varying geometrical parameters; mixing chamber outlet width and its inlet and outlet angle. Woszidlo et al. [13] discovered that increasing the inlet width of the mixing chamber increased output frequency, while rounding the feedback channels reduced bubble formation. According to Slupski and Kara's [14] simulations, feedback channel height affects oscillation frequency up to a point where no further change is observed, whereas increasing feedback channel width decreases frequency.

Tajik et al. [15] and Hossain et al. [16] highlighted that the Coanda surface shape is particularly sensitive to oscillation frequency. Hussain et al. [17] further studied the impact of variation in the aspect ratio of the ribs installed over the Coanda surface to improve the flow performance of the fluidic oscillator. The impact of the location of the ribs over the Coanda surface is yet to be studied. Therefore, this study investigates the effect of the location of the ribs placed on the Coanda surface of the fluidic oscillator. Three different designs are examined to determine how these variations impact performance parameters, such as oscillation frequency, dimensionless pressure drop, frequency–pressure ratio, jet deflection angle–pressure ratio, and frequency jet deflection–pressure ratio (FDPR). The objective is to identify the fluidic oscillator design with the highest frequency and jet deflection/spreading angle (FDPR).

2. Numerical Setup and Geometric Details

The fluidic oscillator's flows are described by compressible continuity, momentum, and energy equations. Favre averaging is used for velocity, temperature, enthalpy, and internal energy, while Reynolds averaging is for density and pressure. The key equations are as follows:

2.1. Continuity Equation

$$\frac{\partial(\overline{\rho})}{\partial t} + \frac{\partial\left(\overline{\rho}\widetilde{u}_i\right)}{\partial x_i} = 0 \tag{1}$$

where $\widetilde{u}_i$ are the density-weighted average velocity components, x_i are the spatial coordinates, and $\overline{\rho}$ is the mean density.

2.2. Momentum Equation

$$\frac{\partial\left(\overline{\rho}\widetilde{u}_i\right)}{\partial t} + \frac{\partial\left(\overline{\rho}\widetilde{u}_i\widetilde{u}_j\right)}{\partial x_j} = -\frac{\partial\overline{P}}{\partial x_i} + \frac{\partial\left[2\overline{\nu}_T\overline{S_{ij}} - \overline{\rho u_i'' u_j''}\right]}{\partial x_j} \tag{2}$$

Here, $\overline{P}$ is mean pressure, $\overline{\nu}_T$ is the temperature-dependent kinematic viscosity, which is calculated by Sutherland's law [18] by the following Equation (3):

$$\mu_{(T)} = \mu_0 \left(\frac{T}{T_0}\right)^{3/2} \left(\frac{T_0 + S_1}{T + S_1}\right) \tag{3}$$

where μ_0 (reference viscosity) = 1.72×10^{-5} kg/m-s and T_0 (reference temperature) and S_1 (effective temperature) are 273.16 K and 110.56 K, respectively.

2.3. Energy Equation

$$\begin{aligned}\frac{\partial}{\partial_t}\left[\overline{\rho}\left(\widetilde{e}+\frac{\widetilde{u}_i\widetilde{u}_i}{2}\right)\right. &+\left.\left(\frac{\overline{\rho u_i'' u_i''}}{2}\right)\right]+\frac{\partial}{\partial x_j}\left[\overline{\rho u}_j\left(\widetilde{h}+\frac{\widetilde{u}_i\widetilde{u}_i}{2}\right)+\widetilde{u}_j\frac{\overline{\rho u_i'' u_i''}}{2}\right]\\ &=\frac{\partial}{\partial x_j}\left[-k\frac{\partial\widetilde{T}}{\partial x_j}-\overline{\rho u_j'' h''}+\overline{t_{ji}u_i''}-\overline{\rho u_j''\frac{1}{2}u_i'' u_i''}\right]\\ &+\frac{\partial}{\partial x_j}\left[\widetilde{u}_i\left(2\overline{v}_T\overline{S}_{ij}-\overline{\rho u_i'' u_j''}\right)\right]\end{aligned} \tag{4}$$

Here, $\widetilde{e}$ is the specific internal energy and $\widetilde{h}$ is the specific enthalpy.

2.4. Turbulence Model

The eddy viscosity model relates Reynolds stresses to mean strain rates through turbulent viscosity (μ_t). The Shear Stress Transport (SST) k–ω model is used for this purpose, which is effective both near and away from walls. The turbulent viscosity for SST k–ω is presented in Equation (5):

$$\mu_t=\frac{\rho k}{\omega}\frac{1}{max\left(\frac{1}{\alpha^*},\frac{F_2 S}{a_1\omega}\right)} \tag{5}$$

where F_2 is the blending function, S is the strain rate magnitude, α^* is the correction factor for a low Re to dampen the turbulent viscosity to appropriate levels, and a_1 is the constant.

2.5. Discretization Schemes and Boundary Conditions

ANSYS Fluent (version 2021) is used to simulate 2D unsteady compressible turbulent flow to solve the Reynolds-averaged Navier–Stokes (RANS) equations. The convective terms for momentum, turbulent kinetic energy, and specific dissipation rates are solved using a second-order upwind scheme. The pressure and velocity are coupled using the SIMPLE algorithm. A fully implicit second-order scheme is used for time stepping. Inlet boundary conditions are set with an inlet velocity of 55.8 m/s. Initially, a uniform velocity distribution is assumed.

The computational setup runs for 10,000 time steps (0.05 s) with a time step size of 5×10^{-6} s to achieve a fully developed oscillating jet. The time step size was selected based on the Courant–Friedrichs–Lewy (CFL) condition, $CFL = \frac{u\,\Delta t}{\Delta x}$, where u is the inlet velocity, Δt is the time step size, and Δx is the spatial mesh size. To ensure stability, we aimed for a CFL number of 1. For the inlet velocity of 55.8 m/s and mesh size of approximately 0.0003 m, a time step size of approximately 5×10^{-6} s ensures a CFL number of 1. Data is saved over another 0.05 s, running for 10,000 time steps to analyze bi-stable oscillation.

2.6. Geometric Details

The SWJ oscillator's geometry matches the previous study [17,19] and includes a mixing chamber, an outlet nozzle, and two feedback channels. The length scale is represented by the exit nozzle throat size (D). The width of the exit nozzle throat is 6.35 mm, while the width of the feedback channel and the mixing chamber is 7.43 mm and 21.52 mm, respectively. In this study, we are studying smooth case oscillators and three ribbed oscillators, as shown in Figure 1. The first oscillator with ribs placed over the Coanda surface called the "full ribs case", has four equal-sized square ribs evenly spaced along the entire Coanda surface. The second ribbed case geometry, the "upper ribs case", has only two equal-sized square ribs located on the upper half of the Coanda surface. Lastly, the third ribbed case geometry, the "lower ribs case", includes two equal-sized square ribs positioned on the lower half of the Coanda surface. The square rib's side length is 0.25D.

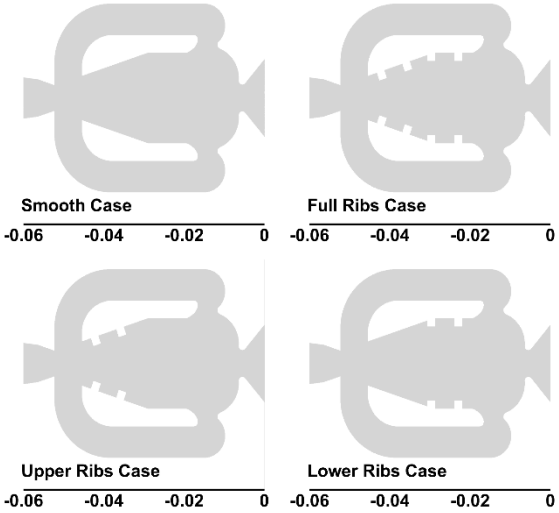

Figure 1. All cases used in the present study.

The performance parameter used in this study is the frequency jet deflection–pressure ratio (FDPR) [19] and is defined as the following:

$$FDPR = \frac{f_e/f_s * \theta_e/\theta_s}{\left(\Delta p_e/\Delta p_s\right)^{1/3}} \quad (6)$$

3. Mesh Sensitivity and Model Validation

3.1. Mesh Sensitivity

To verify the domain discretization, a mesh sensitivity analysis was conducted. Three different meshes were created as shown in Figure 2, using the exit nozzle throat diameter as a key parameter. For this study, the fluidic oscillator's exit nozzle throat diameter (6.35 mm) was considered critical while generating the 2D mesh. Near the fluidic oscillator's wall, the boundary layer is modeled with 20 normal to the wall layers. These layers have a growth rate of 1.1, and the first layer is 0.0127 mm thick (D/500).

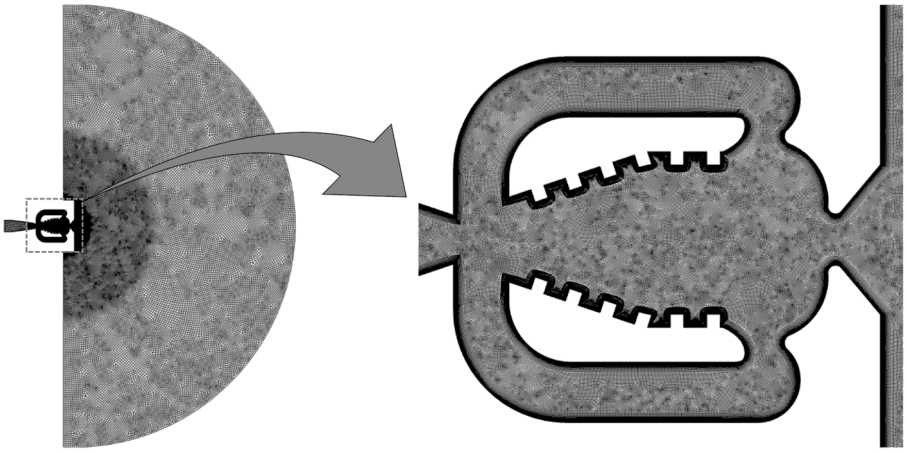

Figure 2. Full domain and oscillator (zoomed) mesh used in the present study.

Three spheres with radii of 8D (50.8 mm), 20D (127 mm), and 100D (635 mm) were employed to enhance the mesh. The element sizes for the outer layers were set to D/5 (1.27 mm) and D/2.5 (2.54 mm) to regulate the element size in the computational region. For the inner sphere, the coarse mesh, labeled N20, included 20 elements along the exit nozzle, with an element size of D/20 (0.3175 mm). The normal mesh, N40, and the fine mesh, N60, used element sizes of D/40 (0.15875 mm) and D/60 (0.10583 mm), respectively.

FFT analysis results as are shown in Figure 3 indicated that the frequencies for N20, N40, and N60 meshes were 340, 355, and 358 Hz, respectively. The frequency results became consistent for the normal and fine meshes, showing only a 0.84% variation. Therefore, the N40 mesh was chosen for further analysis based on these frequency results.

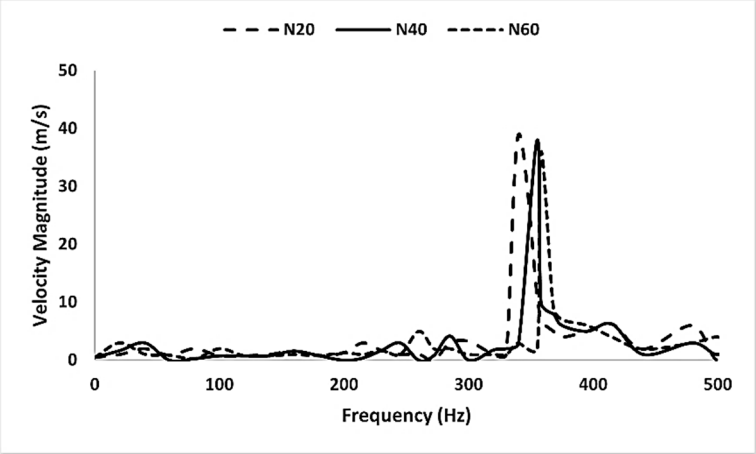

Figure 3. FFT analysis of velocity measurements at sampling point (6 mm and 0 mm) for various computational meshes.

3.2. Model Validation

Table 1 compares the frequency results from the experimental study and previous 2D numerical study with those from the present study. The percentage error shows that the present 2D numerical model accurately predicts the oscillation frequency of the fluidic oscillator, similar to the previous 2D numerical model [18] and experimental study [20]. The relative errors are 1.2% and 2.6%, respectively, indicating that the present numerical model is reliable.

Table 1. Model validation.

Ref.	Analysis Type	Oscillation Frequency	Error
Slupski et al. [20]	Experimental	346 Hz	-
Alam and Kara [18]	2D Numerical	350 Hz	1.2%
Present Study	2D Numerical	355 Hz	2.6%

4. Results and Discussion

The oscillation frequency and deflection angle of the jet leaving from the fluidic oscillator are the two key factors in the cooling of hot surfaces. The oscillation frequency affects how uniformly the surface is cooled, while the jet deflection angle influences the coverage area of the hot surface that is being cooled. Additionally, pressure loss is an important factor in the flow performance of the fluidic oscillator.

4.1. Impact of Location of Ribs on Frequency

The oscillation frequency of the jet exiting the oscillator is an important flow and thermal performance factor. As evident from Figure 4a, the introduction of ribs enhances the oscillation frequency from 355 Hz (smooth case) to 820 Hz (full ribs case). In the case of ribs installed over the Coanda surface, the full ribs case has the highest frequency of 820 Hz, and the upper ribs case has the lowest frequency of 780 Hz. When ribs are installed only on the upper part of the Coanda surface, a separation bubble with a large size as compared to full ribs and lower ribs case, is formed in the mixing chamber, as shown in Figure 4b. The size of the separation bubble formed in the mixing chamber influences the frequency because it affects the jet's switching from one side to the other. A larger separation bubble provides more resistance to the jet's flipping, which lowers the oscillation frequency. On

the other hand, the small size bubble allows the jet to flip faster and results in higher oscillation frequency.

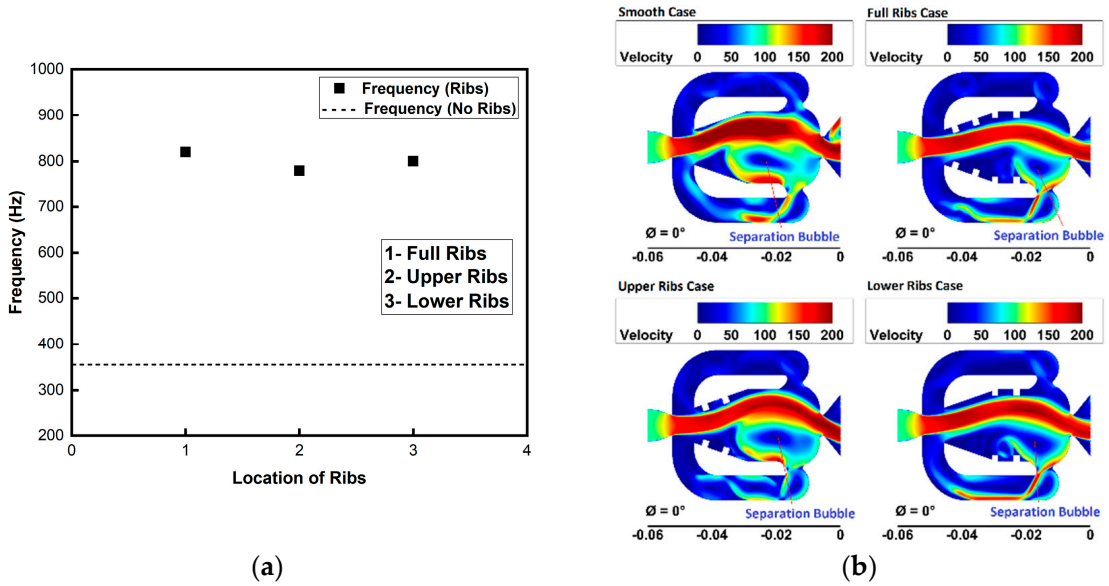

Figure 4. (**a**) Oscillation frequency and (**b**) velocity contours for different locations of ribs.

4.2. Impact of Location of Ribs on Jet Deflection Angle

The jet deflection angle affects the coverage area of the jet impinging on the hot surfaces. The jet deflection angle of the smooth case is the largest at 53.3° when compared to cases with ribs as shown in Figure 5. The large separation bubble in the mixing chamber, shown in Figure 4b, pushes the jet towards the Coanda surface. This causes the jet to leave the oscillator at a larger angle compared to the oscillators with ribs. When comparing cases with ribs, the upper ribs case has the greatest jet deflection angle of 41.5°. This is due to two reasons: first, the formation of a large bubble in the mixing chamber as previously mentioned and second, the absence of ribs in the lower half of the Coanda surface. As a result, the jet is pushed further towards the Coanda surface and exits the oscillator at a wider angle.

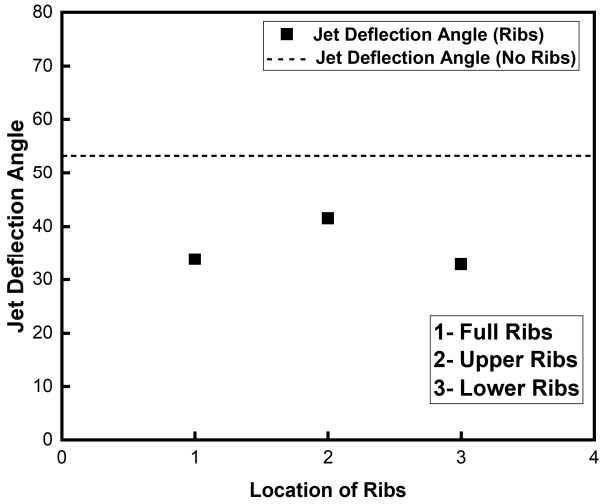

Figure 5. Jet deflection angle for different locations of ribs.

4.3. Impact of Location of Ribs on Pressure Drop

The pressure drop is an important factor in oscillators to determine how well the flow performs. It directly affects the pumping power needed to move the fluid through the

fluidic oscillator. Figure 6 shows how the pressure drop varies with different rib locations on the Coanda surface of the oscillator. The results indicate that the smooth case performs the worst in terms of pressure drop. The oscillator with full ribs has the greatest impact on reducing the pressure drop. This reduction is due to the flow detaching from the Coanda surface because of the ribs, which reduces frictional losses. Among all the oscillators studied, the full ribs case is the most effective in reducing pressure drop.

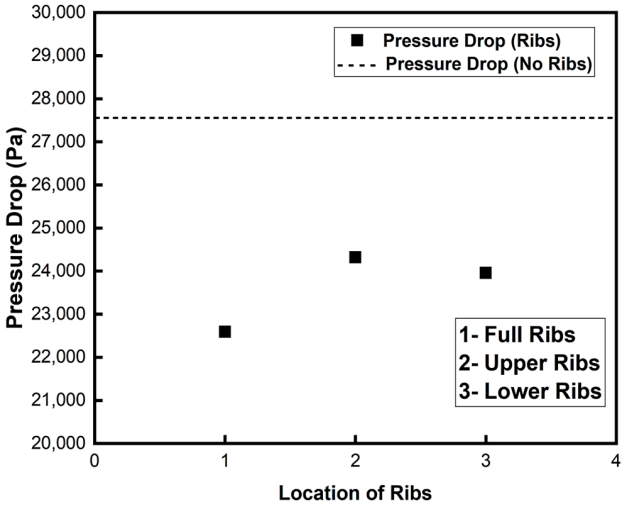

Figure 6. Pressure drop across fluidic oscillator for different locations of ribs.

4.4. Impact of Location of Ribs on Frequency Jet Deflection–Pressure Ratio (FDPR)

The frequency jet deflection–pressure ratio (FDPR) shows the combined impact of the frequency and jet deflection angle versus the pressure ratio across the oscillator.

Figure 7 shows how the performance parameter, FDPR, performs at different locations of ribs on the Coanda surface of the oscillators and for the smooth case oscillator. It is clear from the results that the upper ribs case performs the best in terms of FDPR. As compared to the smooth case, a 76.1% increase is recorded in the value of FDPR for the upper ribs case oscillator. In cases of full ribs and lower ribs, the increase is 58.4% and 45.3%, respectively as compared to the oscillator with no ribs. The increase in FDPR is majorly influenced by the higher jet deflection angle in the upper ribs case as shown in Figure 5. Hence, to utilize the higher combined performance of jet oscillation frequency and jet deflection angle, the upper ribs case provides the best solution.

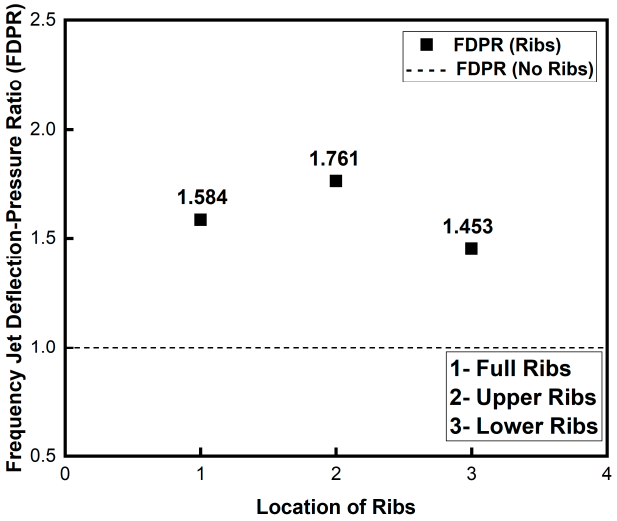

Figure 7. Frequency jet deflection–pressure ratio (FDPR) for different locations of ribs.

5. Conclusions

The present study focused on the effect of rib placement on the Coanda surface within a fluidic oscillator, aiming to understand how these modifications influence jet characteristics such as oscillation frequency, deflection angle, and pressure drop. The introduction of ribs on the Coanda surface markedly increased the oscillation frequency of the jet. The highest frequency observed was 820 Hz in the full ribs case, significantly higher than the 355 Hz frequency of the smooth surface case. However, the presence of ribs also resulted in a decrease in the jet deflection angle. The smooth surface case exhibited the largest deflection angle at 53.3°, whereas the full ribs case had a reduced angle of 33.8°. The upper ribs case achieved a moderate deflection angle of 41.5°, attributed to the formation of a large separation bubble and the absence of ribs on the lower half of the Coanda surface.

Regarding pressure drop, the study found that adding ribs to the Coanda surface significantly reduced the pressure drop within the fluidic oscillator. The full ribs case demonstrated the most considerable reduction in pressure drop, enhancing flow performance by reducing frictional losses due to flow detachment caused by the ribs. The FDPR analysis shows that oscillators with upper ribs significantly outperform smooth case oscillators, achieving a remarkable 76.1% increase in FDPR. Oscillators with full ribs and lower ribs also exhibit notable improvements, though to a lesser extent. The enhanced FDPR in the upper ribs case is mainly attributed to the greater jet deflection angle, indicating that this configuration offers the best solution for the enhancement of the combined performance of jet oscillation frequency and deflection angle.

Author Contributions: Conceptualization, L.H. and M.M.K.; methodology, L.H. and M.M.K.; software, L.H.; validation, L.H.; formal analysis, L.H. and M.M.K.; investigation, L.H. and M.M.K.; resources, M.M.K.; data curation, L.H. and M.M.K.; writing—L.H. and M.M.K.; writing—review and editing, L.H. and M.M.K.; visualization, L.H. and M.M.K.; supervision, M.M.K.; project administration, M.M.K.; funding acquisition, L.H. All authors have read and agreed to the published version of the manuscript.

Funding: This research received no external funding.

Institutional Review Board Statement: Not applicable.

Informed Consent Statement: Not applicable.

Data Availability Statement: The original contributions presented in the study are included in the article, further inquiries can be directed to the corresponding author.

Conflicts of Interest: The authors declare no conflicts of interest.

Nomenclature

SWJ	Sweeping jet	Δp_e	Pressure drop across ribbed (enhanced) oscillator
D	Oscillator exit nozzle throat diameter	Δp_s	Pressure drop across smooth oscillator
FDPR	Frequency jet deflection–pressure ratio	FFT	Fast Fourier transform
f_e	Frequency of ribbed (enhanced) oscillator	URANS	Unsteady Reynolds-averaged Navier–Stokes
f_s	Frequency of smooth oscillator	SST	Shear Stress Transport
θ_e	Jet deflection angle of ribbed (enhanced) oscillator	μ_t	Turbulent viscosity
θ_s	Jet deflection angle of smooth oscillator		

References

1. Raghu, S. Fluidic Oscillators for Flow Control. *Exp. Fluids* **2013**, *54*, 1455. [CrossRef]
2. Wassermann, F.; Hecker, D.; Jung, B.; Markl, M.; Seifert, A.; Grundmann, S. Phase-Locked 3D3C-MRV Measurements in a Bi-Stable Fluidic Oscillator. *Exp. Fluids* **2013**, *54*, 1487. [CrossRef]
3. Bobusch, B.C.; Woszidlo, R.; Bergada, J.M.; Nayeri, C.N.; Paschereit, C.O. Experimental Study of the Internal Flow Structures inside a Fluidic Oscillator. *Exp. Fluids* **2013**, *54*, 1559. [CrossRef]
4. Stouffer, R. Oscillating Spray Device. U.S. Patent 4,151,955, 1 May 1979.
5. Greenblatt, D.; Whalen, E.A.; Wygnanski, I.J. Introduction to the Flow Control Virtual Collection. *AIAA J.* **2019**, *57*, 3111–3114. [CrossRef]

6. Schmidt, H.J.; Woszidlo, R.; Nayeri, C.N.; Paschereit, C.O. Separation Control with Fluidic Oscillators in Water. *Exp. Fluids* **2017**, *58*, 106. [CrossRef]
7. Raman, G.; Raghu, S. Cavity Resonance Suppression Using Miniature Fluidic Oscillators. *AIAA J.* **2004**, *42*, 10–13. [CrossRef]
8. Madadkon, H.; Fadaie, A.; Nili-Ahmadabadi, M. Experimental and Numerical Investigation of Unsteady Turbulent Flow in a Fluidic Oscillator Flow Meter with Extraction of Characteristics Diagrams. *Modares J. Mech. Eng.* **2012**, *12*, 30–42.
9. Lacarelle, A.; Paschereit, C.O. Increasing the Passive Scalar Mixing Quality of Jets in Crossflow with Fluidics Actuators. *J. Eng. Gas Turbines Power* **2012**, *134*, 021503. [CrossRef]
10. Zhou, W.; Yuan, L.; Liu, Y.; Peng, D.; Wen, X. Heat Transfer of a Sweeping Jet Impinging at Narrow Spacings. *Exp. Therm. Fluid Sci.* **2019**, *103*, 89–98. [CrossRef]
11. Hussain, L.; Khan, M.M. Recent Progress in Flow Control and Heat Transfer Enhancement of Impinging Sweeping Jets Using Double Feedback Fluidic Oscillators: A Review. *J. Heat Transf.* **2022**, *144*, 120802. [CrossRef]
12. Bobusch, B.C.; Kr, O.; Paschereit, C.O. Numerical Investigations on Geometric Parameters Affecting the Oscillation Properties of a Fluidic Oscillator. In Proceedings of the 21st AIAA Computational Fluid Dynamics Conference, San Diego, CA, USA, 24–27 June 2013; pp. 1–15.
13. Baghaei, M.; Bergada, J.M. Fluidic Oscillators, the Effect of Some Design Modifications. *Appl. Sci.* **2020**, *10*, 2105. [CrossRef]
14. Woszidlo, R.; Ostermann, F.; Nayeri, C.N.; Paschereit, C.O. The Time-Resolved Natural Flow Field of a Fluidic Oscillator. *Exp. Fluids* **2015**, *56*, 125. [CrossRef]
15. Slupski, B.J.; Kara, K. Effects of Geometric Parameters on Performance of Sweeping Jet Actuator. In Proceedings of the 34th AIAA Applied Aerodynamics Conference, Washington, DC, USA, 13–17 June 2016; pp. 1–13.
16. Tajik, A.; Kara, K.; Parezanovic, V. Sensitivity of a Fluidic Oscillator to Modifications of Feedback Channel and Mixing Chamber Geometry. *Exp. Fluids* **2021**, *62*, 250. [CrossRef]
17. Hossain, M.A.; Prenter, R.; Agricola, L.M.; Lundgreen, R.K.; Ameri, A.; Gregory, J.W.; Bons, J.P.; Researcher, P. Effects of Roughness on the Performance of Fluidic. In Proceedings of the 55th AIAA Aerospace Sciences Meeting, Grapevine, TX, USA, 9–13 January 2017.
18. Alam, M.; Kara, K. The Influence of Exit Nozzle Geometry on Sweeping Jet Actuator Performance. *Fluids* **2022**, *7*, 69. [CrossRef]
19. Hussain, L.; Khan, M.M.; Ahmad, N. Flow Performance Enhancement of a Fluidic Oscillator Through the Integration of Rectangular Ribs on Coanda Surface. *J. Fluids Eng.* **2024**, *146*, 111301. [CrossRef]
20. Slupski, B.J.; Tajik, A.R.; Parezanović, V.B.; Kara, K. On the Impact of Geometry Scaling and Mass Flow Rate on the Frequency of a Sweeping Jet Actuator. *FME Trans.* **2019**, *47*, 599–607. [CrossRef]